Molla, M.M., and Paul, M.C. (2012) *LES of non-Newtonian physiological blood flow in a model of arterial stenosis.* Medical Engineering and Physics, 34 (8). pp. 1079-1087. ISSN 1350-4533.

http://eprints.gla.ac.uk/68803/

Deposited on: 28 August 2012

LES of non-Newtonian physiological blood flow in a model of arterial stenosis

M. M. Molla *and M. C. Paul [†]

School of Engineering, University of Glasgow,

Glasgow G12 8QQ, UK

Abstract

Large Eddy Simulation (LES) is performed to study the physiological pulsatile transition-to-turbulent non-Newtonian blood flow through a 3D model of arterial stenosis by using five different blood viscosity models: (i) Power-law (ii) Carreau (iii) Quemada (iv) Cross and (v) modified-Casson. The computational domain has been chosen is a simple channel with a biological type stenosis formed eccentrically on the top wall. The physiological pulsation is generated at the inlet of the model using the first four harmonic series of the physiological pressure pulse (Loudon and Tordesillas [1]). The effects of the various viscosity models are investigated in terms of the global maximum shear rate, post-stenotic re-circulation zone, mean shear stress, mean pressure, and turbulent kinetic energy. We find that the non-Newtonian viscosity models enlarge the length of the post-stenotic re-circulation region by moving the reattachment point of the shear layer separating from the upper wall further downstream. But the turbulent kinetic energy at the immediate post-lip

*Present address: Department of Mechanical & Manufacturing Engineering, University of Manitoba, Winnipeg, 3RT 5V6, Canada

†Corresponding author: E-mail:Manosh.Paul@glasgow.ac.uk, Tel:+44 (0)141 330 8466, Fax:+44 (0)141 330 4343

of the stenosis drops due to the effects of the non-Newtonian viscosity. The importance of using LES in modelling the non-Newtonian physiological pulsatile blood flow is also assessed for the different viscosity models in terms of the results of the dynamic subgrid-scale (SGS) stress Smagorinsky model constant, C_s, and the corresponding SGS normalised viscosity.

Keywords: Arterial stenosis, LES, Non-Newtonian model, Physiological flow

1 Introduction

Arterial stenosis is commonly found in the arteries of patient who have vascular disease. Stenosis is formed by the deposition of cholesterol and other lipids beneath the intima of the arterial wall, which then reduces the cross-sectional area of artery and changes the blood flow from laminar to turbulent. The hemodynamic factors such as wall pressure and shear stress play an important role in damaging and weaken the internal wall of the artery at the post-stenotic turbulent region. For example, the high wall shear stresses associated with turbulence have strong influences in causing endothelial damages of vessel (Fry [2]). In some cases, they overstimulate platelet thrombosis which then accelerate atherosclerosis as reported in Stein *et al.* [3]. On the other hand, the intimal thickening that causes the remodelling of the vessel wall relates to the presence of the low shear stresses at the throat of the stenosis, Ku *et al.* [4]. Furthermore, the non-invasive diagnostic device which is commonly used in the clinical practice to determine the severity of stenosis depends on the intensity of the local turbulent pressure fluctuations as a potential source of arterial murmurs, Lees and Dewey [5].

Over the past few decades much attentions have been paid in the investigation of the stenotic flow by assuming that the blood is a Newtonian and homogeneous fluid. However, blood is a non-Newtonian incompressible viscoelastic fluid (Fung [6], pp.53) and at a shear rate above about $100s^{-1}$ the blood viscosity tends towards an asymptotic value. Moreover, if the shear rates fall below that asymptotic level, the viscosity of blood increases and the non-Newtonian properties of blood being exhibited (Berger and Jou [7]), especially when the shear rates drop below $10s^{-1}$ (Huang *et al.* [8]).

Very few studies found in the literature that relate to the investigation of the non-Newtonian blood flow in arterial stenosis. Most relevant recent papers are Tu and Delville [9], Neofytou and Drikakis [10], Hron *et al.* [11], and Valencia and Villanueva [12]. They applied various blood viscosity models and found the effects of the blood rheology on the wall shear stresses and pressures. However, all these

studies have been conducted for the laminar flow. To the best of our knowledge, there is no single numerical/computational paper that has looked into the details of the transition-to-turbulent of the non-Newtonian blood flow in an arterial stenosis. Therefore, the general aim of this paper is to investigate, by using LES, how the choice of the various non-Newtonian viscosity models, discussed in § 2.2, affect the process of transition of the blood flow through stenosis. In particular, we aim to investigate the effects of the blood viscosity models on the shear stress and pressure on the arterial walls and the turbulence downstream of the stenosis by giving insight into the relevant pathological consequences.

Most recent work of Paul *et al.* [13] and Molla *et al.* [14] show the novelty of the LES approach in studying transitional flow in bio-fluid mechanics. The pulsatile turbulent blood flow through a model of arterial stenosis have been investigated in these papers assuming that the blood is a Newtonian fluid. In the current paper, we extend our investigation into the non-Newtonian regime as we believe this will give more accurate insight into the transition of the blood flow in the stenosis. The model geometry (Fig. 1) studied in [13, 14] gives a fairly reasonable representation of an asymmetric arterial stenosis and remains same here. The geometry consists of a 3D channel with a one-sided cosine shape stenosis which is formed on the upper wall at $x/L = 0$ by using

$$\frac{x}{L} = 1 - \frac{\delta_c}{2}\left(1 + \cos\frac{y\pi}{h}\right), \quad -L \le y \le L \tag{1}$$

where δ_c is fixed to $\frac{1}{2}$, which results in a 50% reduction of the cross-sectional area at the centre of the stenosis. Note that the length of the stenosis is twice the channel height $(L = 5mm)$ and it is centred $5L$ downstream of the channel inlet and $15L$ from the channel outlet. In the figure, we use x, y and z to represent the vertical, streamwise and spanwise coordinates, respectively.

4

2 Governing equations

The filtered Navier-Stokes equations of motion for non-Newtonian fluid flow may be written as

$$\frac{\partial u_j}{\partial x_j} = 0, \tag{2}$$

$$\frac{\partial \rho u_i}{\partial t} + \frac{\partial \rho u_i u_j}{\partial x_j} = -\frac{\partial p}{\partial x_i} + \frac{\partial}{\partial x_j}\left[\mu(|\dot{\gamma}|)\left(\frac{\partial u_i}{\partial x_j} + \frac{\partial u_j}{\partial x_i}\right)\right] - \frac{\partial \tau_{ij}}{\partial x_j}, \tag{3}$$

where $u_j = (u, v, w)$ are the filtered velocity vectors along the coordinate system, $x_j = (x, y, z)$, respectively; p is pressure; t is time; and $\rho = 1.05 \times 10^3$ kg·m^{-3} is the fluid density. The blood viscosity, $\mu(|\dot{\gamma}|)$, depends on the shear rate, $\dot{\gamma}_{ij} = \frac{1}{2}\left(\frac{\partial u_i}{\partial x_j} + \frac{\partial u_j}{\partial x_i}\right)$, and its magnitude defined as $|\dot{\gamma}| = \sqrt{2\dot{\gamma}_{ij}\dot{\gamma}_{ji}}$ (Tu and Delville [9]). When blood is treated as a Newtonian fluid, its viscosity tends to a constant value which is denoted by $\mu_\infty = 3.45 \times 10^{-3}$ Pa·s. While for a non-Newtonian model constitutive relations used for the apparent viscosity of the blood are presented in § 2.2. The subgrid-scale stress terms, τ_{ij}, are modelled by employing the Smagorinsky model [15],

$$\tau_{ij} - \frac{1}{3}\delta_{ij}\tau_{kk} = -2\nu_{sgs}S_{ij} = -2(C_s\triangle)^2|S|S_{ij}, \tag{4}$$

where C_s is the Smagorinsky constant obtained via the localized dynamic model of Piomelli-Liu [16] by clipping the negative values of the constant C_s to zero; $\triangle = \sqrt[3]{\triangle x\triangle y\triangle z}$ is the filter width; and $|S| = \sqrt{2S_{ij}S_{ij}}$ is the magnitude of the large scale strain rate tensor, S.

2.1 Boundary conditions

An analytic solution of the momentum equation (3) in the streamwise direction is obtained by taking the pressure gradient as a Fourier series in time as shown in Loudon and Tordesillas [1]. The solution of the streamwise velocity takes the following form, only real part of this is used to generate physiological pulsatile profile at the inlet.

$$v(x,t) = 4V\frac{x}{L}\left(1 - \frac{x}{L}\right) + A\sum_{n=1}^{N}\frac{iM_nL^2}{\mu\alpha^2n}$$

$$\left[\cosh(\alpha\sqrt{in}\frac{x}{L}) - \frac{\cosh(\alpha\sqrt{in}) - 1}{\sinh(\alpha\sqrt{in})}\sinh(\alpha\sqrt{in}\frac{x}{L}) - 1\right]e^{i(n\omega t + \phi_n)}, \quad\quad (5)$$

where the bulk velocity, V, depends on the flow Reynolds number defined as $Re = \frac{VL}{\nu}$; L is the height of the channel; and $\alpha = L\sqrt{\frac{\rho\omega}{\mu}}$ is the Womersley number which gives the ratio between the unsteady and viscous forces where ω is the frequency of the unsteady flow. When Womersley number is relatively small, the viscous forces usually dominate flow. However, unsteady inertia forces take an important role in the physiological flow when $\alpha > 10$ as reported in by Ku [17]. As our aim is to investigate the transition of the physiological pulse in the model stenosis, a value of α greater than 10 is required in the simulations. We therefore used $\alpha = 10.5$. Moreover, to control the magnitude of the physiological pulse at the peak the amplitude, A, is fixed to 0.4 which is determined based on the peak Reynolds number of 2000. The values used for the pulsatile coefficient, M_n, and the corresponding phase angle, ϕ_n, for the first four harmonics (i.e. $N = 4$) of the physiological flow are given in Table 1, Womersley [18].

The inlet pulsatile velocity profile derived from the relation above (5) is now presented in Fig. 2 in order to show the temporal and spatial variation of the pulsation imposing at the inlet of the model. As seen in frames (a,b), the velocity initially rises with time to a peak occurring at the systolic phase ($t/T = 0.25$) then drops rapidly up to the mid-location of the pulse at the diastolic phase. The growth of the velocity in rest of the period is modest as the heart relaxes, and the left ventricle in heart fills with blood during the diastole. Interesting features also noticed in frame (c), especially it shows that the pattern of the parabolic-type profiles of the velocity changes from its peak with the regime of the reverse flow (where the velocity is negative) occurring close to the channel walls during the diastolic phase (e.g. at $t/T = 0.5$, 0.625 and 0.75).

At the outlet a convective boundary condition is used while no-slip boundary conditions for both the lower and upper walls of the model since the walls are assumed to be rigid. For the spanwise boundaries, periodic boundary conditions are applied for modelling the spanwise homogeneous flow.

2.2 Non-Newtonian blood viscosity models

Five different widely used non-Newtonian constitutive relationships for the blood viscosity model against the shear rate investigated in the paper are summarised below.

2.2.1 Power-law model

The Power-law model which was proposed by Walburn and Schneck [19] takes into account of the haematocrit which is the volume percentage of red blood cells in whole blood. This viscosity model is given by

$$\mu(|\dot{\gamma}|) = k|\dot{\gamma}|^{n-1}, \tag{6}$$

where $k = 14.67 \times 10^{-3}$ and $n = 0.7755$ are the model constants.

2.2.2 Carreau model

Carreau [20] proposed a four-parameter non-Newtonian viscosity model which is given by

$$\mu(|\dot{\gamma}|) = \mu_\infty + (\mu_0 - \mu_\infty)[1 + (\lambda\dot{\gamma})^2]^{(n-1)/2}, \tag{7}$$

where $\mu_0 = 0.056$ Pa.s is the blood viscosity at a zero shear rate, $\lambda = 3.131$ is the time constant associated with the viscosity that changes with the shear rate, and $n = 0.3568$.

2.2.3 Quemada model

This model was developed by Quemada [21] to predict the viscosity of concentrated systems based on the shear rate and haematocrit. The viscosity model is given by

$$\mu(|\dot{\gamma}|) = \mu_p \left(1 - \frac{1}{2}\frac{k_0 + k_\infty\sqrt{|\dot{\gamma}|/\gamma_c}}{1 + \sqrt{|\dot{\gamma}|/\gamma_c}}\phi\right)^{-2}, \tag{8}$$

where $\mu_p = 1.2 \times 10^{-3}$ Pa.s is the viscosity of plasma and for haematocrit $\phi = 0.45$. The values of the model parameters used are $\gamma_c = 1.88\text{s}^{-1}$, $k_\infty = 2.07$ and $k = 4.33$.

2.2.4 Cross model

Cross [22] proposed a shear rate dependent viscosity model as

$$\mu(|\dot{\gamma}|) = \mu_\infty + \frac{(\mu_0 - \mu_\infty)}{\left[1 + \left(\frac{\dot{\gamma}}{\gamma_c}\right)^n\right]}, \tag{9}$$

where $\mu_0 = 0.0364$ Pa.s is the blood viscosity at a very low shear rate, $\gamma_c = 2.63\text{s}^{-1}$, which is the reference shear rate and $n = 1.45$ is the model constant.

2.2.5 Modified casson model

Casson viscosity model originally introduced by Casson [23] for the prediction of the flow behaviour of pigment-oil suspension takes the following form:

$$\mu(|\dot{\gamma}|) = \frac{\left[\sqrt{\tau_0} + \sqrt{\eta_c \dot{\gamma}}\right]^2}{\dot{\gamma}}. \tag{10}$$

However, Merrill *et al.* [24] reported that the rheological properties of human blood at a shear rate ranging from 0.1 to $1.0 s^{-1}$ are consistent with the Casson model, but they deviate to some extent in the range of $1 - 40 s^{-1}$. Bate [25] believed that the blood flow through tubes is best described by the Casson model in the shear rate range of $15 - 6400 s^{-1}$. Therefore, for large-diameter vessels, like arteries, a modified and more-general Casson model was formulated by Gonzalez and Moraga [26]:

$$\mu(|\dot{\gamma}|) = \left(\sqrt{\eta_c} + \frac{\sqrt{\tau_0}}{\sqrt{\lambda} + \sqrt{\dot{\gamma}}}\right), \tag{11}$$

where $\eta_c = 3.45 \times 10^{-3}$ Pa.s is the Casson viscosity, $\tau_0 = 2.1 \times 10^{-2} s^{-1}$ is the yield stress and $\lambda = 11.5 s^{-1}$ is a constant when the shear rate tends to zero.

3   Numerical methods and assessments

An in-house developed finite volume LES code with collocated grid arrangement for velocity and pressure has been used to solve the governing equations (2-3) with the appropriate boundary conditions in § 2.1. The code is second order accurate in both space and time, and fully implicit. Further details on the numerical algorithm

including the discretisation and solution processes could be found in [13, 14, 27] and the relevant references therein. Validation of the code with the experimental results of Ahmed and Giddens [28] have already been performed in Molla *et al.* [14], and overall a very good agreement received - this validation exercise will not be repeated in the paper. However, it is important to check the mesh resolution to be used in the simulations is adequate enough to resolve the transient flow downstream of the stenosis. To this end, a grid independence test has been conducted for the Newtonian model with a constant value of the viscosity. Three LES with three different grid arrangements as shown in Table 2 and a coarse DNS have been performed with a constant timestep of 10^{-3}sec.

The results are compared in Fig. 3 in terms of the time-mean streamwise velocity, $< v > /V$ (top), and the turbulent kinetic energy, $\frac{1}{2} < u_j'' u_j'' > /V^2$ (bottom). The number of streamwise grid points upstream of the stenosis is always fixed at 50 while the rest of the grid points are distributed nonuniformly within and downstream of the stenosis. The grid is significantly refined in the near-wall region in order to accurately resolve the wall shear stress while it is uniform in the spanwise direction. The agreement found in particular for the mean streamwise velocity is quite good indeed, so the mean flow is well resolved by the grids used in the four simulations. However, some sensitivities exist in the turbulent results especially towards the immediate post stenotic region. This might be understood by the fact that only the resolved scale flows are computed in LES by the grid resolution, so a totally grid independence to the computed turbulent random fluctuations is not expected in LES, and it is adequate to prove in LES that the primary flow features (mean velocities) do not vary significantly by the choice of the grid. The dependence remains apparent until the grid resolution becomes fine enough that the LES starts to qualify as DNS. Based on the satisfactory agreement above the grid arrangement of $50 \times 200 \times 50$ (Case 1) has been used for all other simulations.

9

4 Results and discussion

4.1 Viscosity models vs. shear rate

The relationship between the apparent shear rates and viscosity for the above mentioned five non-Newtonian blood viscosity models along with the Newtonian viscosity model is presented in Fig. 4. In general, the viscosity of blood produced by the non-Newtonian models for low shear rates (e.g. $< 100s^{-1}$) is higher than that of the Newtonian model. In the Newtonian model the blood viscosity is constant which is shown by the solid line. More specifically, the blood viscosity in the Power-law model at low shear rates increases but decreases at large shear rates - the variation with the shear rate is linear. However, the limitation of the Power-law model is that it fails to describe the viscosity of blood at very low or high level of shear rates. On the other hand, the viscosity in the Carreau and modified-Casson models tends to the asymptotic constant viscosity, μ_∞, at the shear rate $\dot{\gamma} > 10^4 s^{-1}$. The Quemada and Cross models exhibit the non-Newtonian properties of blood at shear rate $\dot{\gamma} < 10^2 s^{-1}$. Particularly, in the Cross model the viscosity asymptotically matches the constant viscosity at the shear rates $\dot{\gamma} > 10^2 s^{-1}$ but the Quemada model shows the asymptotic nature below the constant viscosity μ_∞.

Milnor [29] argued that the blood viscosity using the above mentioned viscosity models becomes infinite at a very lowest rate of shear, which is impossible to occur practically. To get a true effect of the non-Newtonian blood viscosity, following Johnston et al. [30], the lowest shear rate used in the whole computation is $0.1s^{-1}$ as can be seen in Fig. 4. Furthermore, the necessity for using the non-Newtonian model is made clear by observing the range of the global maximum shear rate ($|\dot{\gamma}|$), plotted in Fig. 5, for the different non-Newtonian models. From this figure it is clear that the global maximum shear rates lie within the range of the non-Newtonian shear rate, $\dot{\gamma} < 10^2 s^{-1}$, during some part of the time cycle where the non-Newtonian properties of blood would play an important role in the process of transition. The effects in predicting turbulence quantities at the post-stenosis regime are discussed

in the following section.

4.2 Effects of the viscosity models

Fig. 6 depicts the post-stenotic re-circulation zone in terms of the mean streamlines for the Newtonian and different non-Newtonian models. As seen, the length of the re-circulation region is enlarged to the post-stenotic region in the non-Newtonian models, which is an alarming condition, at the pathological point of view, that the blood in the post-stenosis region is re-circulated for a long time and stagnant in this region which could potentially cause the blood clot or thrombosis leading to stroke and heart attack.

In Table 3, comparisons of the point of separation of the shear layer from the nose of the stenosis and its position of re-attachment on the upper-wall at the post-stenosis for the different models are given. The separation in the Newtonian model starts early, as point of separation (PA) is recorded at about -0.09382 which is an upstream location of the nose; while late separation is predicted by all the non-Newtonian models and their PA occurs at about the same post-nose location. Comparing all the re-attachment (RA) points, it is clear that the Newtonian model under-predicts the regime of the post-stenosis recirculation of blood, while the Carreau model has an overall maximum prediction of the recirculation regime.

Mean shear stress, $\tau_{xy}/\rho V^2$, distributions at the upper wall, centreline and lower wall are compared in Fig. 7(a-c) respectively for the different viscosity models. At the upper wall the stress drop is predicted higher in the case of non-Newtonian model than that of the Newtonian model, in particular the Power-law model predicts the maximum stress drop at the nose of the stenosis. In terms of magnitude, the stress drop in the Power-law model is about -0.07730 which is about 32% higher than the Newtonian model for which it is -0.05869. Interestingly, the upper-wall stress drop in all the models occurs at a same streamwise location, $y/L = -0.12505$. The difference between the non-Newtonian and Newtonian models of the shear distribution is also distinguishable in the post-stenotic turbulent region. However, in the laminar

11

region the differences are very small and towards the further downstream region the upper wall shear stresses for the non-Newtonian models are always smaller than the case of Newtonian model.

In the centreline, the shear stress drop predicted by the non-Newtonian models is also higher than that of the Newtonian model. But, in this frame the Carreau model shows the highest drop at the post-stenosis. In the pathological context, the shear stress drop usually stimulates the re-modelling of arterial wall and as a results the percentage of the arterial stenosis increases. Thus, the predicted shear stress drop by the non-Newtonian models would have more impact on the vessel reshaping at the stenosis regime. Furthermore, as reported by Fry [2], the potential endothelium damage to the inner side of the post-stenotic blood vessel is caused by the acute shear stress in the excess of about 30 Pa. The shape of the blood cells is also affected by the alternation of the magnitude of the shear stress from 10 Pa to 250 Pa which causes the red blood cells to deform gradually toward a smooth ellipsoidal shape (Sutera and Mehrjardi [31]). The peak lower wall shear stress, in Fig. 7(c), is predicted to be about 91 Pa in the dimensional form. Therefore, the simulation results evidence that the extreme rise of the shear stress in the lower wall and the oscillating shear stresses in the post-stenosis zone, predicted by the non-Newtonian models, will have more influence in causing potential damage to the materials of blood cells ([31]) and also to the endothelium or inner side of the post-stenotic blood vessel ([2]).

In Fig. 8(a-c) corresponding mean pressure, $p/\rho V^2$, are compared at the upper wall, centreline and lower wall respectively. The blood pressure, predicted by all the viscosity models, shows a sudden drop at the centre of the stenosis in the upper wall. In terms of its dimensional value, it is around 23.13 mmHg (or 3083.31 Pa) drop, which could potentially be a cause of hypotension of a patient with stenosis in the artery ([32]). Pressure along the centreline and the lower wall also drops, and particularly at the downstream of the stenosis the pressure drops by 24.49 mmHg (3264.69 Pa) and 17.69 mmHg (2357.83 Pa) respectively for the Newtonian blood

model.

Although the differences in the pressure distributions between the Newtonian and non-Newtonian models are clearly visible, among the non-Newtonian models it is very small. The pressure drop predicted at the throat of the stenosis is slightly higher in the case of the Newtonian model than the case of non-Newtonian models. Further downstream the pressure for the non-Newtonian models is higher than the case of Newtonian model. Additionally, the pressure drop in the post-stenosis links with the potential source of stroke or heart attack since the low blood pressure causes inadequate blood supply to the heart, brain and other vital organs [32]. We can argue that the Newtonian model over-estimates the risk of forming these diseases.

Fig. 9(a-b) illustrates the centreline mean kinetic energy (MKE), $\frac{1}{2} < u_j u_j > /V^2$, and the turbulent kinetic energy (TKE), $\frac{1}{2} < u''_j u''_j > /V^2$, for the different models. In frame (a), the MKE is almost identical at the upstream of the stenosis for all the models, where the flow is laminar. However, at the turbulent region ($1.0 \leq y/L \leq 6.0$) the MKE varies in the non-Newtonian models with a magnitude that is slightly higher in the Carreau and Quemada models compared to the Newtonian model. Significant effects are reported on the results of the turbulent kinetic energy in frame (b). The peak of TKE in the post-stenotic region ($1.0 < y/L < 3.0$) occurs in the Newtonian model, while all the non-Newtonian models produce higher TKE at the downstream ($3.0 < y/L < 9.0$) because of the fact that the physiological oscillation which is reduced by the high viscosity in the non-Newtonian models causes delay in the transition process. Turbulence also has important clinical significances, for example, the TKE in the post-stenotic region could cause damage to the blood-cell materials and to activate platelets in the blood, and subsequently, they could create many pathological diseases (Ku [17]). But, as seen in Fig. 9, prediction of the TKE and the risk factor of diseases associated with the magnitude of the TKE would clearly depend on the viscosity model used in the simulation.

4.3 Effects on the SGS models

It would be interesting now to investigate how the various non-Newtonian viscosity models affect the SGS models used in LES. In this regard, numerical values of the global maximum Smagorinsky dynamic constant C_s, and the normalised SGS viscosity (μ_{sgs}/μ) for the different non-Newtonian models along with the Newtonian model are compared in Table 4. In general, we found that the value of C_s lies within the range of $0.12 - 0.14$, which somewhat shows an agreement with the typical values $(0.1 - 0.2)$ of the Smagorinsky constant usually found in literature for LES of turbulent channel flow. Influence of the various viscosity models on C_s and μ_{sgs}/μ are clearly seen in Table 4. For example, the maximum value of C_s is obtained by the power-law non-Newtonian model, while some of the other non-Newtonian models show an acceptable number with the Newtonian model. However, important to note that, the location where the maximum of C_s occurs in the post-stenotic region varies with the viscosity models though firmly localised within $1.85 < y/L < 2.81$. The same can be seen in μ_{sgs}/μ where the downstream position also varies with the viscosity models. Moreover, the Newtonian model has the largest SGS dissipation, and among the various non-Newtonian models the SGS dissipation in the Quemada model is maximum.

5 Conclusion

Non-Newtonian physiological flow in a model of arterial stenosis has been investigated by using the LES technique. The global maximum shear rate obtained in the various viscosity models lies within the non-Newtonian range, i.e. less than $100s^{-1}$, which clearly indicated the necessity of using the non-Newtonian blood viscosity model in the investigation. Effects of the various viscosity models on the wall shear stress and pressure distributions have been presented in the paper. We found that the shear stress drop in the upper-wall, where the stenosis is located, is higher in the non-Newtonian models than that of the Newtonian models. Relevant

14

pathological consequences of this predicted result have been highlighted in the paper. For example, re-modelling of the arterial wall because of the acute stress drop will be more influenced by the non-Newtonian models than the Newtonian model. In contrast, the pressure drop in the post-stenosis is predicted slightly smaller in the non-Newtonian models, so the risk of potential heart attack or stroke would be under-estimated by the non-Newtonian models.

Turbulent kinetic energy predicted by the non-Newtonian models differs from the Newtonian model and is particularly high in the non-Newtonian models. Pathologically, this result is also important as the turbulence influences to cause potential damage to the materials of blood cells and activate platelets. We also found that the post-stenotic re-circulation region extends slightly further downstream for the non-Newtonian models, which again increases the possibility of blood clot or thrombosis. Overall, the flow distribution is significantly changed due to the non-Newtonian nature of the blood which also changes the value of the SGS model constant and the rate of dissipation.

Although a simple model of the arterial stenosis is considered for the simulation, the results presented in the paper would be of great interest to medical doctors and help them to understand the important roles of the non-Newtonian blood flow transition in a real-life biological stenosis. It is also true that a stenosis in a real biological vessel would not always form symmetrically. Therefore, our results would be particularly useful for a biological stenosis which is non-uniform and asymmetric.

References

[1] C. Loudon, A. Tordesillas, The use of the dimensionless Womersley number to characterize the unsteady nature of internal flow, *J. Theor. Biol.*, 191 (1998) 63–78.

[2] D. L. Fry, Acute vascular endothelial changes associated with increased blood velocity gradients, *Circulation Res.*, 22 (1968) 165–197.

[3] P. Stein, F. J. Walburn, H. N. Sabbah, Turbulent stresses in the region of aortic and pulmonary valves, *J. Biomechanics Engineering*, 104 (1982) 238–244.

[4] D. N. Ku, D. P. Giddens, C. K. Zarins, S. Glagov, Pulsatile flow and atherosclerosis in the human carotid bifurcation, *Atherosclerosis*, 5 (1985) 293–302.

[5] R. S. Lees, C. F. Dewey, Phonoangiography: a new noninvasive diagnostic method for studying arterial disease, *Proceedings of the National Academy of Science*, 67(2),October (1970) 935–942.

[6] Y. C. Fung, *Biomechanics: Circulation,*, 2nd edition, Springer,1997.

[7] S. A. Berger, L.-D. Jou, Flows in stenotic vessels, *Annu. Rev. Fluid Mechanics*, 32 (2000) 347–382.

[8] C. R. Huang, W. D. Pan, H. W. Chen, A. L. Copley, Thixotropic properties of whole blood from healthy human subjects, *Biorheology* , 24 (1987) 795–801.

[9] C. Tu, M. Delville, Pulsatile flow of non-Newtonian fluids through arterial stenosis, *J. Biomechanics*, 29 (7) (1996) 899–908.

[10] P. Neofytou, D. Drikakis, Effects of blood models on flows through a stenosis, *Int. J. Numer. Meth. Fluids*, 43 (2003) 597–635.

[11] J. Hron, J. Malek, S. Turek, A numerical investigation of flows shear-thinning fluids with applications to blood rheology, *Int. J. Numerical Methods in Fluids* , 32 (2000) 863–879.

[12] A. Valencia, M. Villanueva, Unsteady flow and mass transfer in models of stenotic arteries considering fluid-structure interaction, *Int. Communication Heat and Mass Transfer*, 33 (2006) 966–975.

[13] M. C. Paul, M. M. Molla, G. Roditi, Large-eddy simulation of pulsatile blood flow, *Medical Engineering and Physics*, 31 (2009) 153–159.

[14] M. M. Molla, M. C. Paul, G. Roditi, LES of additive and non-additive pulsatile flows in a model arterial stenosis, *Computers Methods in Biomechanics and Biomedical Engineering*, 13 (1) (2010) 105–120.

[15] J. Smagorinsky, General circulation experiment with the primitive equations. i. the basic experiment, *Monthly Weather Rev.*, 91 (1963) 99–164.

[16] U. Piomelli, J. Liu, Large-eddy simulation of rotating channel flows using a localized dynamic model, *Physics of Fluids*, 7(4) (1995) 839–848.

[17] D. N. Ku, Blood flows in arteries, *Annu. Rev. Fluid Mechanics*, 29 (1997) 399–434.

[18] J. R. Womersley, Method for the calculation of velocity, rate of flow and viscous drag in arteries when the pressure gradient is known, *J. Physiology*, 155 (1955) 553–563.

[19] F. J. Walburn, D. J. Schneck, A constitutive equation for whole human blood, *Biorheology*, 13 (1976) 201–210.

[20] P. J. Carreau, Rheological Equation from Molecular Network Theories, *J. Rheology*, 16 (1) (1972) 99–127.

[21] D. Quemada, Rheology of concentrated disperse system III. General features of the proposed non-Newtonian model. Comparison with experimental data, *Rheology Acta*, 17 (1977) 643–653.

[22] M. M. Cross, Rheology of non-Newtonian fluids: A new flow equation for viscoelastic systems, *J. Collied Science*, 20 (1965) 417.

[23] N. Casson, *Rheology of Disperse System*, Pergamon press, London (1959) 84–104.

[24] E. W. Merrill, G. R. Cokelet, A. Britten, R. E. Wells, Non-Newtonian rheology of human blood-effect of fibrinogen deduce by subtraction, *Circulation Reserach*, 13 (1963) 48–55.

[25] H. Bate, Blood viscosity at different shear rates in capillary tubes, *Biorheology*, 14 (1977) 267–275.

[26] H. A. Gonzalez, N. O. Moraga, On predicting unsteady non-Newtonian blood flow, *Applied Mathematics and Computations*, 170 (2) (2005) 909–923.

[27] M. M. Molla, Les of pulsatile flow in the models of arterial stenosis and aneurysm, PhD thesis, July 2009, University of Glasgow, UK.

[28] S. A. Ahmed, D. P. Giddens, Velocity measurement in steady flow through axisymmetric stenosis at moderate Reynolds number, *J. Biomechanics*, 16 (7) (1983) 505–516.

[29] W. R. Milnor, *Hemodynamics*, Williums and Wilkins, Baltimore, 1982, 49-55 .

[30] B. M. Johnston, P. R. Johnston, S. Corney, D. Kilpatrick, Non-Newtonian blood flow in human right coronary arteries: steady state simulations, *J. Biomechanics* , 37 (2004) 709–720.

[31] S. P. Sutera, M. H. Mehrjardi, Deformation and fragmentation of human red blood cells in turbulent flow, *Biophysical J.*, 15 (1975) 1–10.

[32] WebMd, Understanding low blood pressure: Symptoms, diagnosis and treatment, *Heart disease guide*, (2011) http://www.webmd.boots.com/heart–disease/guide/understanding–low–blood–pressure–diagnosis–treatment.

Table 1: Values of M_n and ϕ_n according to Womersley [18].

Number of harmonics (n)	M_n	ϕ_n
1	0.78	0.0113446
2	1.32	-1.4442599
3	-0.74	0.4625122
4	-0.41	-0.2879793

Table 2: Mesh details for the LES and DNS approaches.

Case	approach	N_x	N_y	N_z
1	LES	50	200	50
2	LES	50	250	50
3	LES	70	250	50
4	DNS	70	350	50

Table 3: Point of separation (PS) and re-attachment (RA) point for the different models.

Point	Newtonian	Power-law	Carreau	Quemada	Cross	Mod-Casson
PS	-0.09382	0.1131	0.1131	0.1131	0.1131	0.1131
RA	2.1651	2.4370	2.5082	2.3673	2.4370	2.3673

Table 4: Global maximum values of C_s and the normalised SGS viscosity (μ_{sgs}/μ) for the different models at $t/T = 10.25$ (peak).

Model	C_s	x/L	y/L	z/L	μ_{sgs}/μ	x/L	y/L	z/L
Newtonian	0.12	0.58	1.85	0.67	0.97	0.70	2.44	0.78
Power-law	0.14	0.23	2.81	0.43	0.81	0.79	2.44	0.43
Carreau	0.12	0.58	2.37	0.02	0.72	0.58	2.37	0.02
Quemada	0.13	0.70	2.37	0.28	0.95	0.70	2.37	0.27
Cross	0.12	0.62	2.72	0.35	0.66	0.62	2.72	0.35
Mod-Casson	0.12	0.62	2.51	0.39	0.84	0.54	2.51	0.39
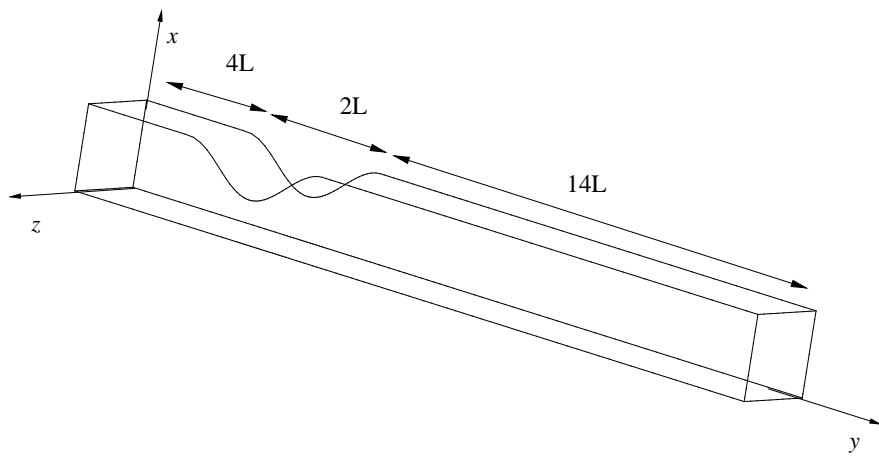
Figure 1: A Schematic geometry of the model with coordinate system.
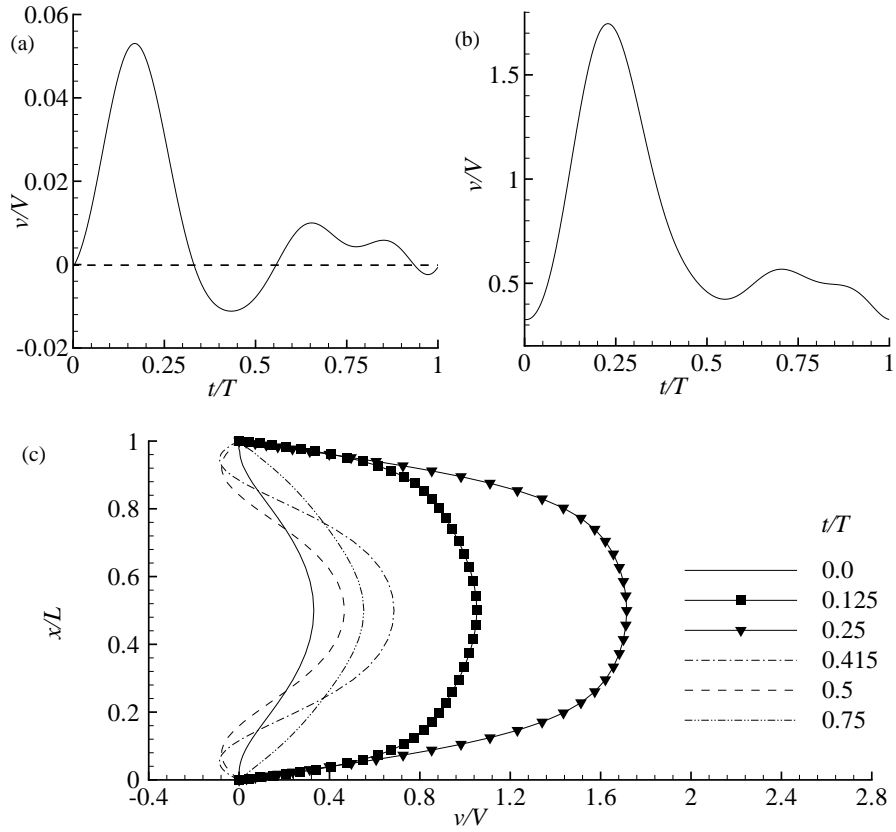
Figure 2: Inlet velocity profile of the physiological pulsation for a time cycle: (a) near the wall, (b) at the centre of the channel and (c) at the different phases.
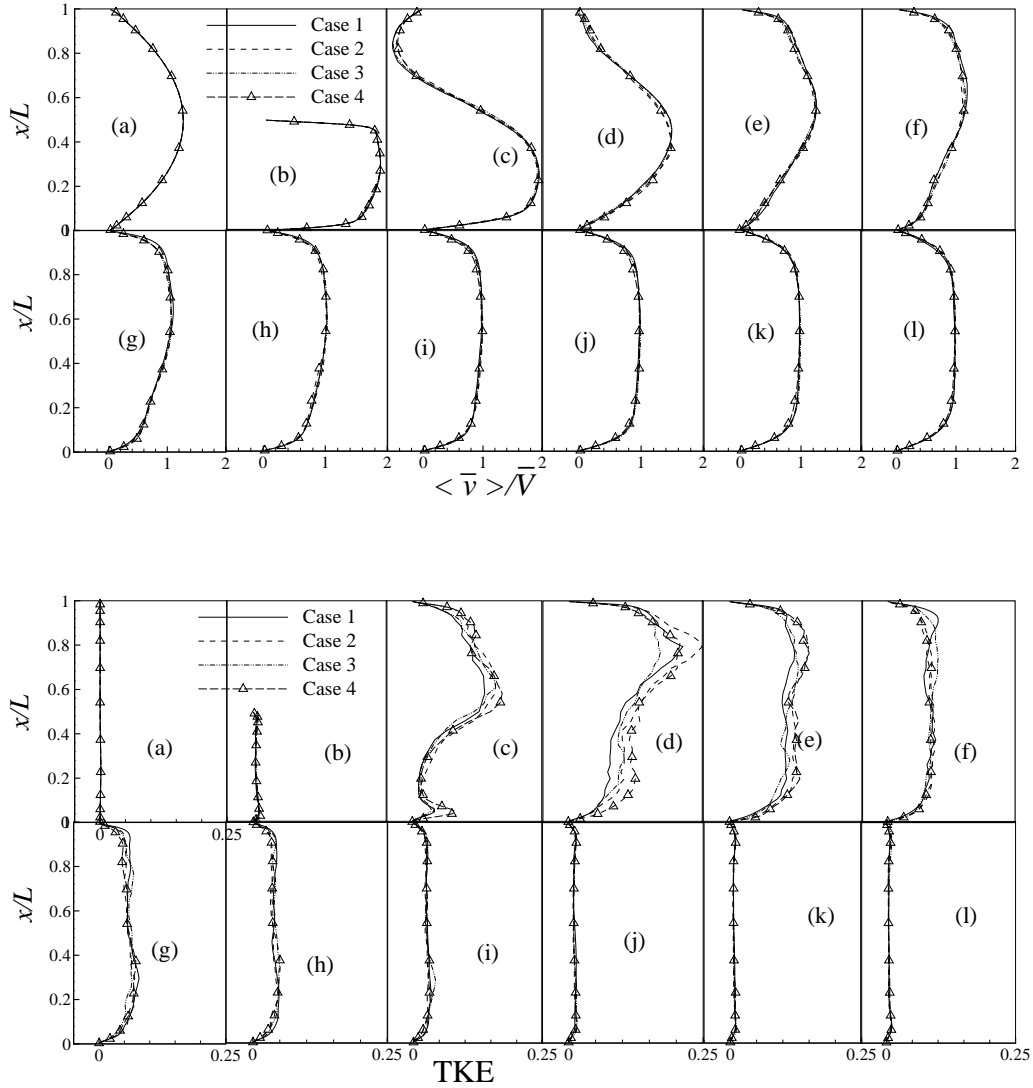
Figure 3: Grid independence test showing on the time-mean streamwise velocity, $< v > /V$, (top) and the turbulent kinetic energy (TKE), $\frac{1}{2} < u_j'' u_j'' > /V^2$, at (a) $y/L =$ inlet, (b) $y/L = 0.0$, (c) $y/L = 1.0$, (d) $y/L = 2.0$,(e) $y/L = 3.0$, (f) $y/L = 4.0$, (g) $y/L = 5.0$, (h) $y/L = 6.0$, (i) $y/L = 8.0$, (j) $y/L = 10.0$, (k) $y/L = 12.0$ and (l) $y/L =$ outlet.
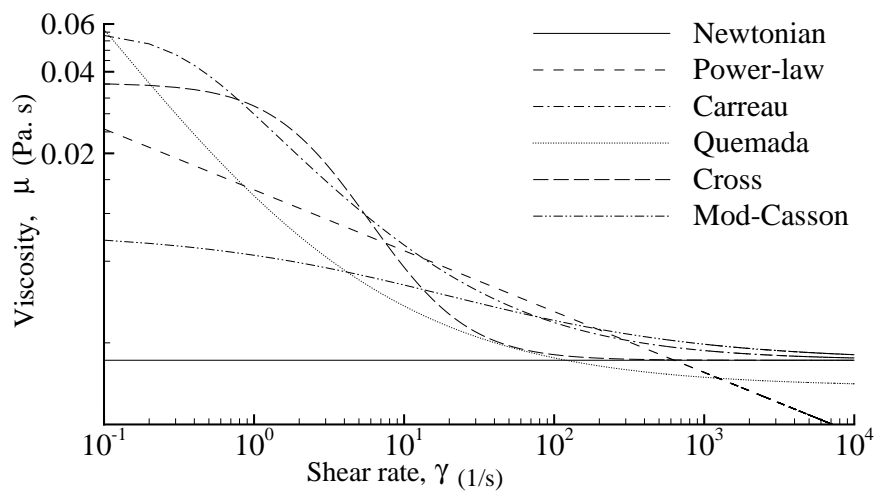
Figure 4: Relations between the shear rate and the apparent blood viscosity for the different models.
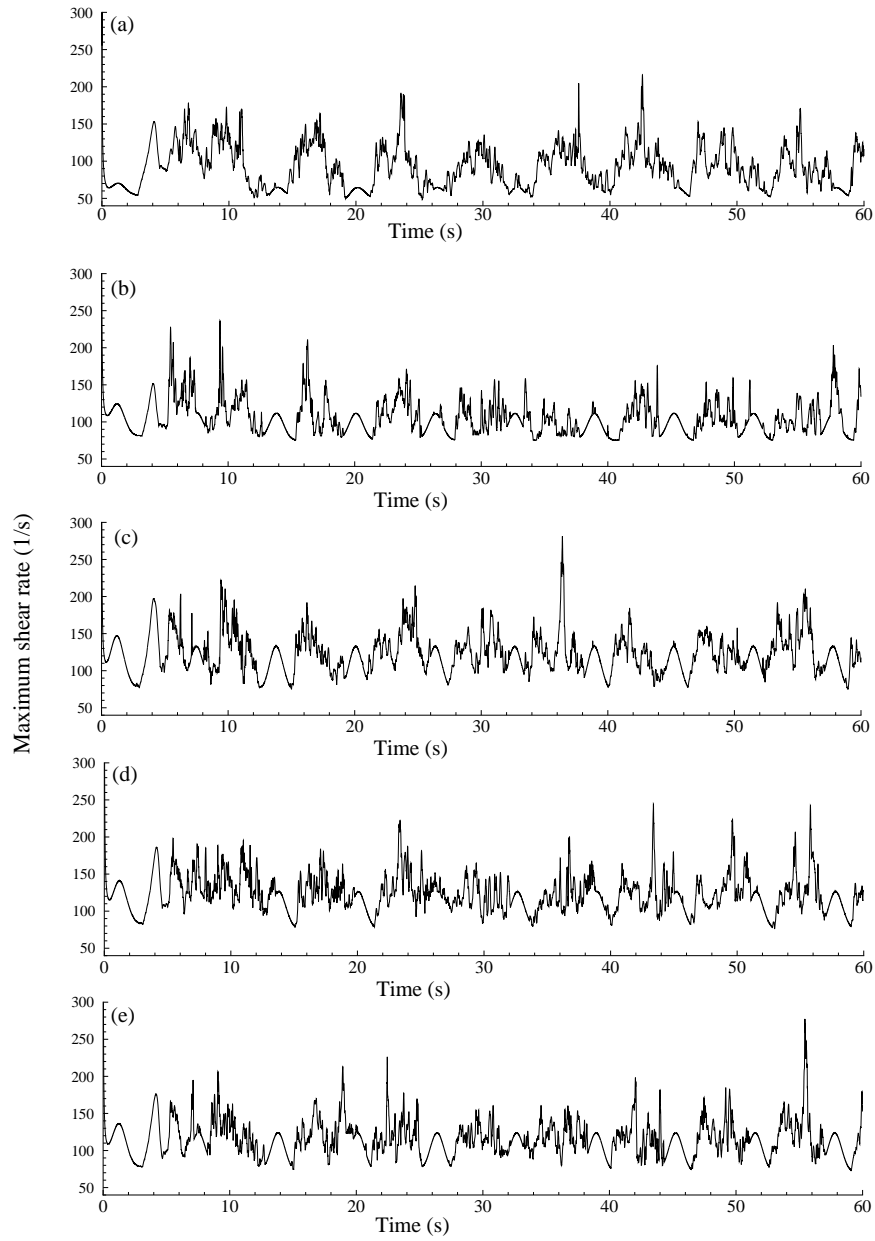
Figure 5: Global maximum shear rate ($|\dot{\gamma}|$) against time for the (a) Power-law (b) Carreau (c) Quemada (d) Cross and (e) modified-Casson models.
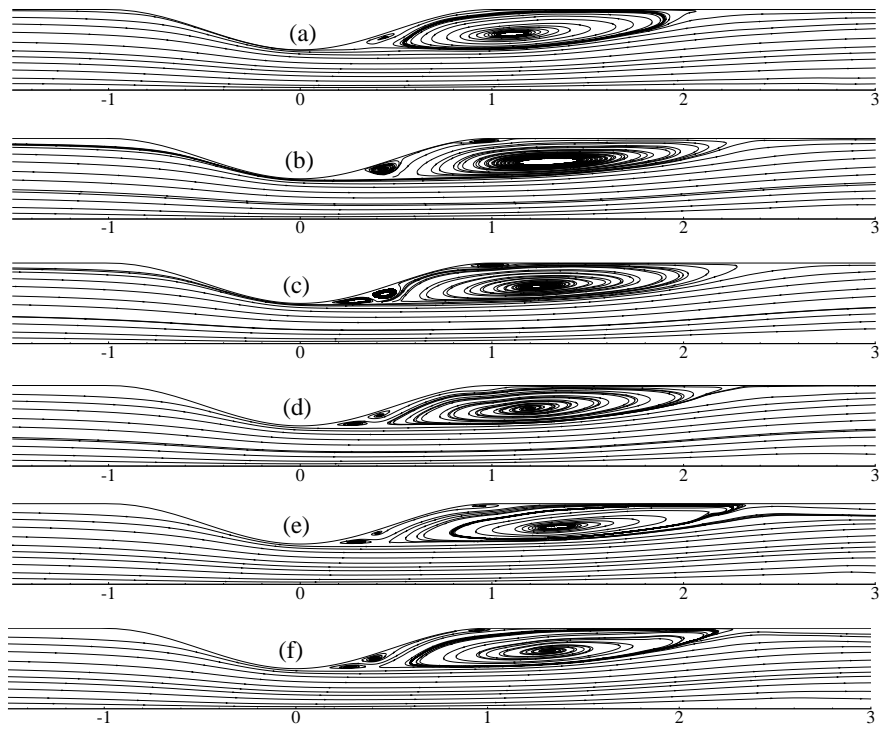
Figure 6: Mean post-stenotic recirculation zone, (a) Newtonian (b) Power-law (c) Carreau (d) Quemada (e) Cross and (f) modified-Casson models.
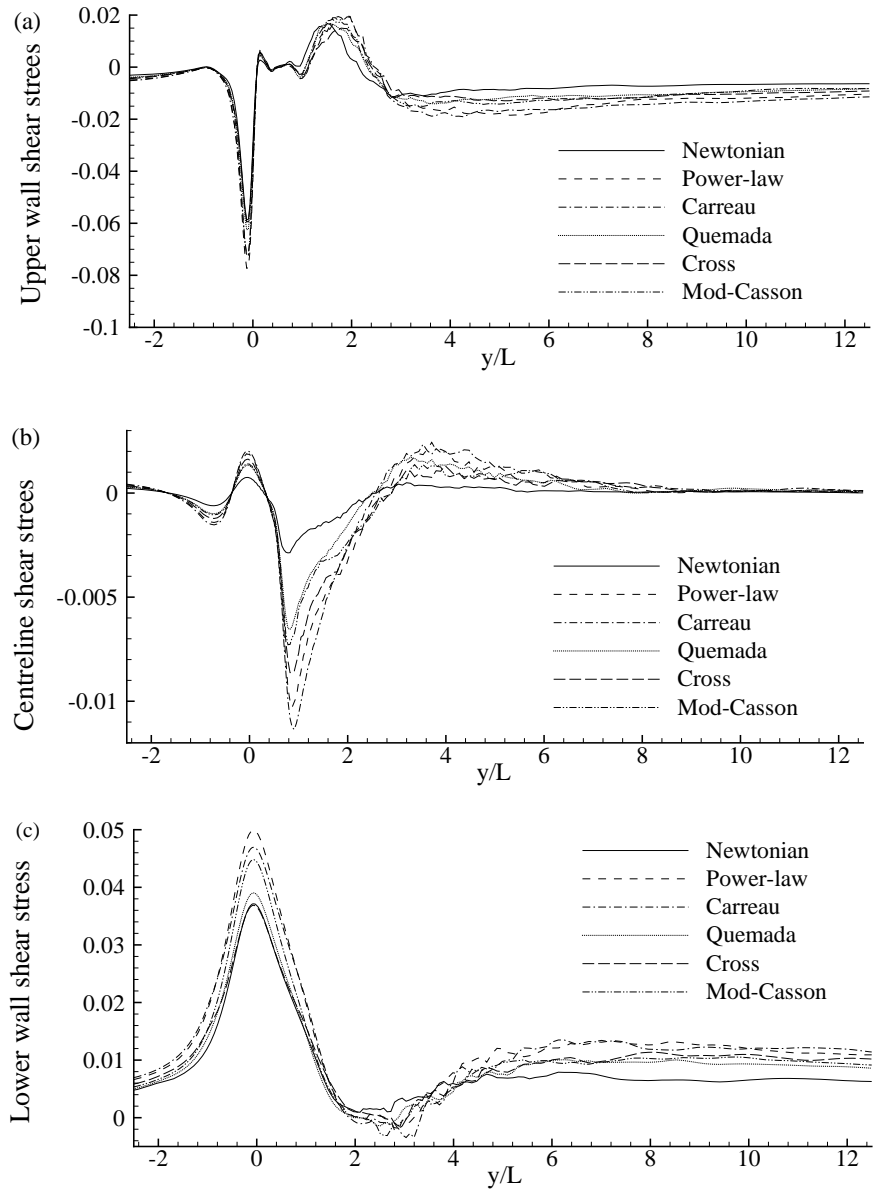
Figure 7: Mean shear stress, $\tau_{xy}/\rho V^2$, at the (a) upper wall (b) centreline and (c) lower wall for the different blood viscosity models.
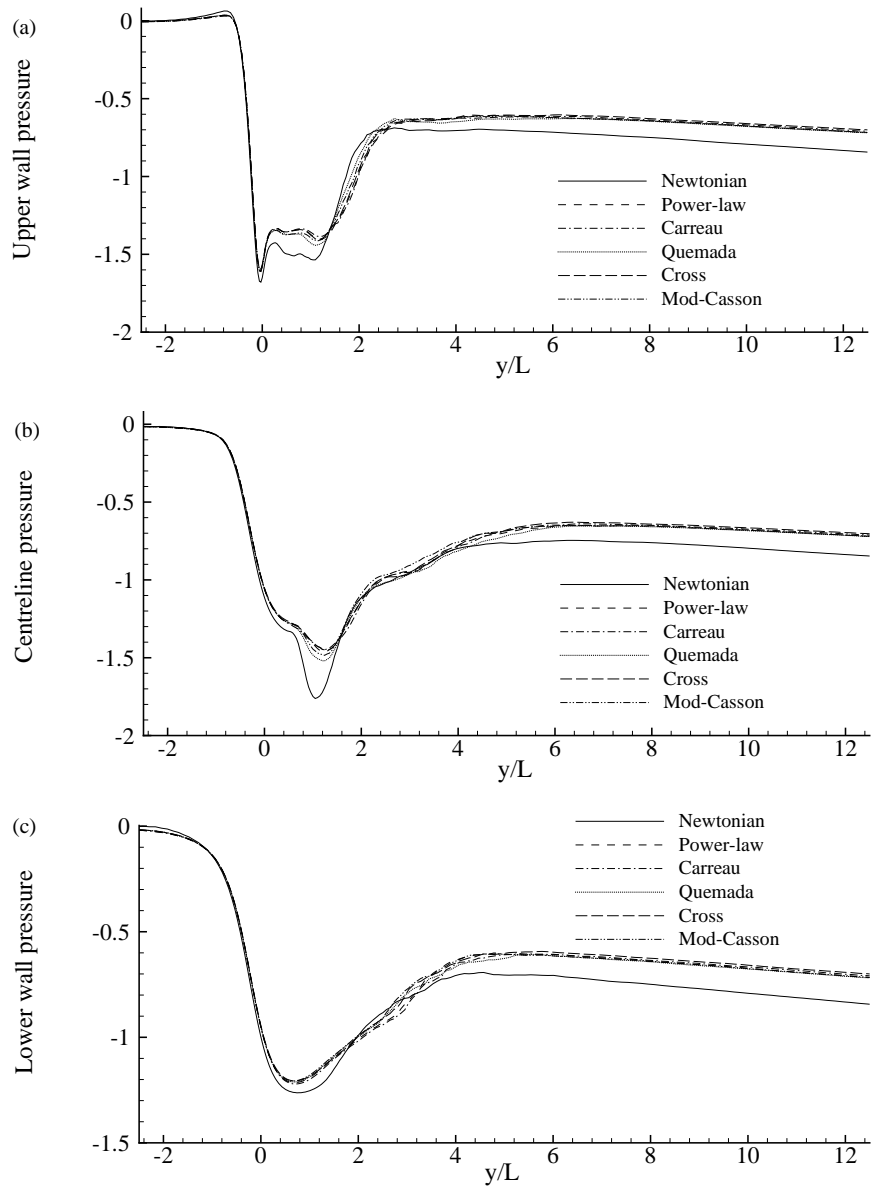
Figure 8: Mean pressure, $p/\rho V^2$ at the (a) upper wall (b) centreline and (c) lower wall for the different blood viscosity models.
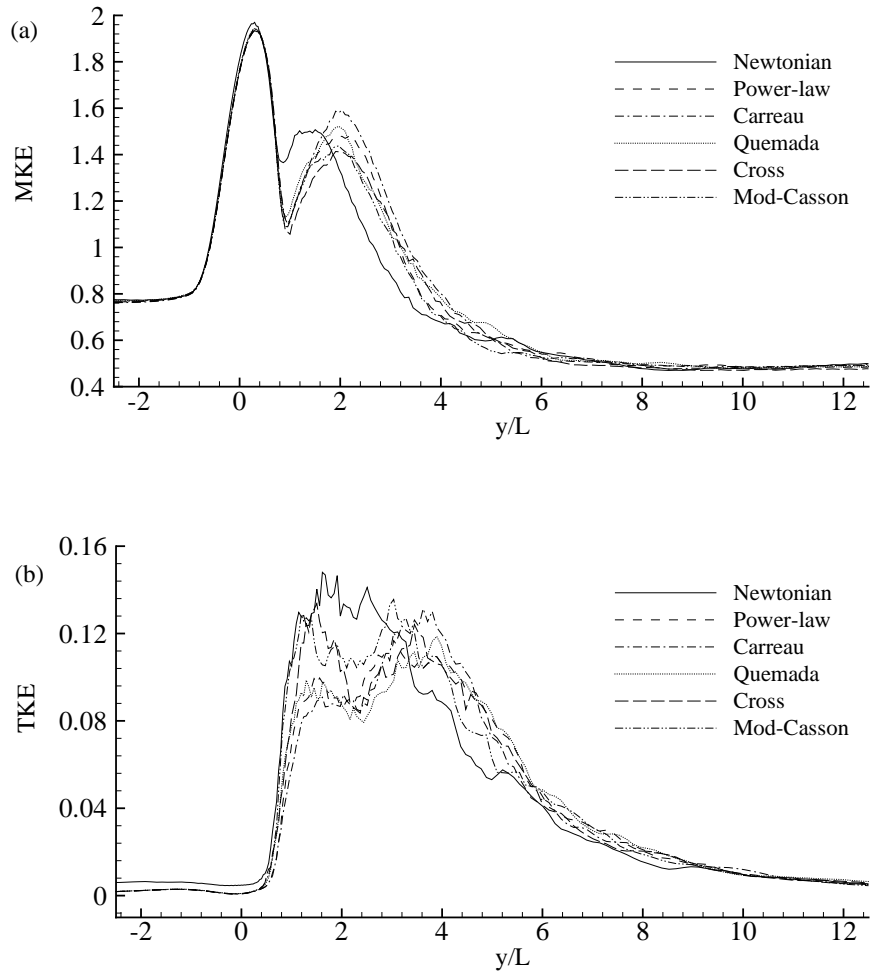
Figure 9: (a) Mean kinetic energy, $\frac{1}{2} < u_j u_j > /V^2$, and (b) turbulent kinetic energy, $\frac{1}{2} < u_j'' u_j'' > /V^2$, at $x/L = z/L = 0.5$ for the different blood viscosity models.